







Surface-normal illuminated pseudo-planar Ge-on-Si avalanche photodiodes with high gain and low noise

FIONA FLEMING,¹  XIN YI,^{1,*}  MUHAMMAD M. A. MIRZA,² XIAO JIN,³ JAROSLAW KIRDODA,² DEREK C. S. DUMAS,² LISA SAALBACH,¹ MRUDUL MODAK,¹ DAVE A. S. MUIR,¹ CHARLIE SMITH,²  CONOR COUGHLAN,² QINGYU TIAN,³  ROSS W. MILLAR,² JOHN P. R. DAVID,³ DOUGLAS J. PAUL,²  AND GERALD S. BULLER¹ 

¹*Institute of Photonics and Quantum Sciences, School of Engineering and Physical Sciences, Heriot-Watt University, Edinburgh, EH14 4AS, UK*

²*James Watt School of Engineering, University of Glasgow, Rankine Building, Oakfield Avenue, Glasgow G12 8LT, UK*

³*Department of Electronic and Electrical Engineering, University of Sheffield, Sheffield, S1 3JD, UK*
**xin.yi@hw.ac.uk*

Abstract: Germanium-on-Silicon (Ge-on-Si) avalanche photodiodes (APDs) are of considerable interest as low intensity light detectors for emerging applications. The Ge absorption layer detects light at wavelengths up to ≈ 1600 nm with the Si acting as an avalanche medium, providing high gain with low excess avalanche noise. Such APDs are typically used in waveguide configurations as growing a sufficiently thick Ge absorbing layer is challenging. Here, we report on a new vertically illuminated pseudo-planar Ge-on-Si APD design utilizing a $2\ \mu\text{m}$ thick Ge absorber and a $1.4\ \mu\text{m}$ thick Si multiplication region. At a wavelength of 1550 nm, $50\ \mu\text{m}$ diameter devices show a responsivity of $0.41\ \text{A/W}$ at unity gain, a maximum avalanche gain of 101 and an excess noise factor of 3.1 at a gain of 20. This excess noise factor represents a record low noise for all configurations of Ge-on-Si APDs. These APDs can be inexpensively manufactured and have potential integration in silicon photonic platforms allowing use in a variety of applications requiring high-sensitivity detectors at wavelengths around 1550 nm.

Published by Optica Publishing Group under the terms of the [Creative Commons Attribution 4.0 License](https://creativecommons.org/licenses/by/4.0/). Further distribution of this work must maintain attribution to the author(s) and the published article's title, journal citation, and DOI.

1. Introduction

Silicon (Si) based photonics have received significant interest and investment in recent years due to their promising potential for producing compact and cost-effective, high-performance photonic integrated circuits (PICs) [1]. This is motivated by the vast array of emerging applications which rely on such PICs, such as high-speed optical communication [2–5], remote sensing [6], light detection and ranging (LiDAR) and 3D imaging-based platforms [7–11]. Avalanche photodiodes (APDs) are highly suited for use in these applications as they can provide a 5 – 10 dB improved sensitivity, compared to basic photodiodes, due to their internal gain (or multiplication factor, M) [12]. The operation of an APD requires a p-n, or, more often, a p-i-n junction which is reverse biased below the avalanche breakdown voltage. Low-intensity incident light can initiate a readily detectable avalanche current via the impact ionization process. Due to the stochastic nature of this impact ionization process, however, this internal gain always comes with the penalty of excess noise factor, F . The relationship between F and M was derived by McIntyre as: $F(M) = kM + (1-k)(2-1/M)$, where $k = \beta/\alpha$ is the ratio of the impact ionization coefficients of

the holes, β , and electrons, α [13]. Despite the excess noise, the gain can reduce the effect of the electronic noise on overall receiver sensitivity. Using an avalanche material, such as silicon, with a small k of 0.02 - 0.1 can result in a higher useful avalanche gain which in turn leads to an improved sensitivity [14].

Very recently, rapid developments in technologies such as free-space optical communications and autonomous unmanned systems have driven the demand for APDs working in the short-wave infrared (SWIR), as there are significant advantages for such systems when working in this spectral region [9,15,16]. One of the main challenges of realizing a high-performance APD on an Si platform operating in the SWIR spectral region is to design and fabricate an efficient absorption region (i.e. with high responsivity and low dark current), since Si has a cut off wavelength of $\lambda \approx 1.1 \mu\text{m}$. The use of germanium (Ge), which has a direct bandgap of $\approx 0.8 \text{ eV}$ at room temperature without strain, in a Separate Absorption and Multiplication APD (SAM-APD) structure, provides a means to absorb SWIR light on a Si-based platform, while utilizing an adjacent Si layer as a low-noise avalanche multiplication region. The device performance, however, is often limited by the 4.2% lattice mismatch between Ge and Si. This mismatch leads to a high number of threading and misfit dislocations, as well as increased surface roughness, all of which tend to result in a larger dark current and reduced compatibility with Si electronics compared to all-Si APDs [17]. Kang *et al.* reported on a $1 \mu\text{m}$ thick Ge absorber in a SAM-APD configuration with a high gain-bandwidth product (GBP) of 340 GHz [18] operating at a wavelength of 1310 nm. Kim *et al.* [19] used a thicker $1.3 \mu\text{m}$ Ge absorber to achieve a unity gain responsivity of 0.35 A/W at 1550 nm and a maximum multiplication of 57. Using selective epitaxial growth techniques, Duan *et al.* demonstrated a responsivity of 0.3 A/W at 1550 nm with a $1 \mu\text{m}$ thick Ge absorber and a gain of 39 [20]. Other groups have used nanostructuring as a means to enhance the absorption in a relatively thin Ge absorber [21]. In the past ten years, waveguide-coupled Ge-on-Si APDs [22–27] have attracted extensive research interest due to the ease of growth of thinner Ge absorbing layers with higher responsivities. Recent work has reported a waveguide device integrated with distributed Bragg reflectors with a unity gain responsivity of $\approx 1.25 \text{ A/W}$ with a maximum M of 14 when operated at 1550 nm wavelength [28]. Shi *et al.* reported a waveguide-coupled Ge/Si impedance resonance APD with a primary responsivity of 0.87 A/W at 1550 nm, dark current of $12 \mu\text{A}$ at 90% of the breakdown voltage and an ultrahigh gain-bandwidth product of 1033 GHz [4].

Most of the previous work on surface-normal illuminated APDs in Ge on Si has involved some form of mesa geometry. Recently, a new pseudo-planar geometry structure, using localized boron implantation, was demonstrated to successfully centralize the very high electric-field in the Si multiplication layer away from the device side-walls in single-photon avalanche diode (SPAD) detectors operated at 1310 nm wavelength [29–32]. Here, we demonstrate the benefits of the pseudo-planar design for a Ge-on-Si APD structure which reduces edge breakdown effects and therefore enables high gain to be achieved. Dual temperature growth techniques [17,33–35] have been shown to provide a way to address the challenges of producing a reliable device design and growing the Ge layer on Si with much greater thickness than the critical thickness due to strain. In this work, we have designed, fabricated and experimentally demonstrated pseudo-planar Ge-on-Si APDs operating at 1550 nm wavelength and at room temperature. A $2 \mu\text{m}$ thick Ge absorption layer enhances the primary responsivity at longer wavelengths, and a $1.4 \mu\text{m}$ Si multiplication region facilitates large gain with low excess noise. The device is grown and fabricated using silicon foundry-compatible processes for low-cost and high-yield mass production, and in this case, 150 mm diameter Si substrates were used. The experimental results demonstrate an APD device with a primary responsivity of 0.41 A/W at 1550 nm, a high M of 101 (≈ 2 times higher than previous Ge-on-Si mesa APD detectors), and a record F of 3.1 at a M of 20. This has allowed the first demonstration of Si-based APDs with a high gain and low excess noise performance at a wavelength of 1550 nm.

2. Device growth, fabrication and structure

Figure 1(a) shows a cross-sectional schematic diagram of the Ge-on-Si SAM-APD structure. The inset of Fig. 1(a) shows the cross-sectional scanning electron microscope image of the Ge-on-Si structure. Due to the thicker 2 μm Ge absorption layer, the pseudo-planar geometry structure was modified slightly to centralize the very high electric-field in the Si region. We used Silvaco TCAD to simulate device electric-field profiles with varying doping densities in a 100 nm thick charge sheet layer. Figure 1(b) shows the electric-field profiles in the centre of a device with a charge sheet layer p-type doping density of $0.8 - 1.1 \times 10^{17} \text{ cm}^{-3}$ and at a reverse bias of 50 V. The optimised charge sheet layer helps to maintain a low electric-field in the Ge layer to avoid ionization in Ge ($< 100 \text{ kV/cm}$). Figure 1(c) shows a self-consistent Poisson-Schrödinger calculation of the band profile at the Ge and Si heterointerface with 0.18%

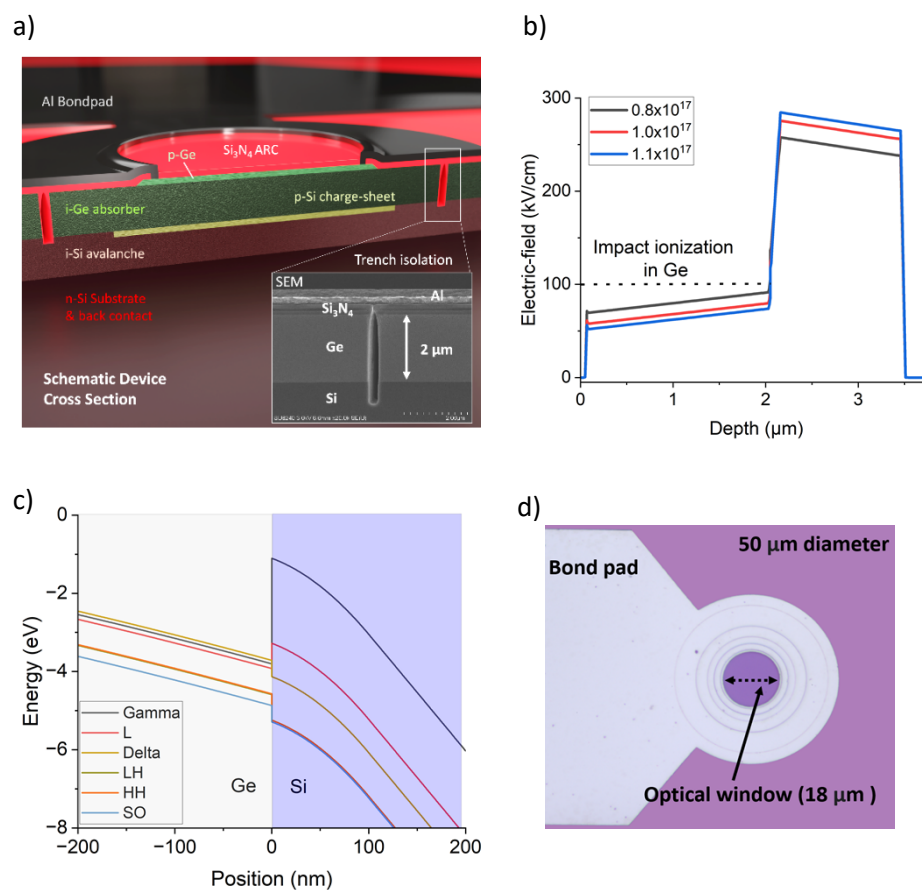


Fig. 1. a) A cross-sectional schematic diagram of an APD device. Inset: cross-sectional scanning electron microscope image of Ge-on-Si structure. b) Electric-field profile simulation for a device structure similar to (a) at a reverse bias of 50 V. The device has a 2 μm Ge absorption layer, a 1.4 μm Si multiplication layer and a 100 nm charge sheet thickness, with three levels of p-type doping of $0.8, 1.0$ and $1.1 \times 10^{17} \text{ cm}^{-3}$. The dashed line indicates the electric-field required for impact ionization in Ge at room temperature. c) A graph of band energy calculation against position at the Ge and Si heterointerface with 0.18% strain in the Ge at a reverse bias of 50 V. d) A microscope image of a new Ge-on-Si device with the bond pad. The device diameter is defined as the boron implantation diameter.

strain in the Ge at a reverse bias of 50 V. Such band alignment allows the photo-generated carriers located in the L-valley of the Ge absorber to be very efficiently injected into the Delta-valley of the Si multiplication layer. Figure 1(d) shows an optical microscope image of a 50 μm diameter Ge-on-Si APD with an optical window diameter of 18 μm . The details of device growth and fabrication can be found in Supplement 1.

3. Experimental results

3.1. Dark and photo-current

The dark currents measured under reverse biased conditions in three different devices are presented in Fig. 2(a). The measured forward bias current of device A is also shown. The forward IV characteristics indicate ideality factors of ≈ 1.2 and a device series resistance of $< 2\text{k}\Omega$. All devices demonstrate clear avalanche breakdown at -55 V (determined when the dark current has reached 100 μA). Compared to the previous generation of Ge-on-Si devices, with a Ge thickness of 1 μm [29,30], the optimization of the structure design and fabrication process has reduced the reverse bias dark current. The dashed line in Fig. 2(a) presents the photocurrent measurement when illuminated with a wavelength of 1550 nm by using a lock-in amplifier to remove the DC dark current. The punch-through voltage is defined as the voltage at which the electric-field depletes the charge sheet region and the absorption region. This is not necessarily the same as the unity avalanche gain point as by the time the electric-field depletes the charge sheet region and the absorption region, the electric-field in the silicon multiplication region is high enough to give rise to significant multiplication. Figure 2(b) shows the secondary ion mass spectroscopy (SIMS) elemental profiles of boron and arsenic. The boron present in the Ge is at the sensitivity limit of the technique and similarly the arsenic in the Si is close to the detection limit at around $5 \times 10^{15} \text{ cm}^{-3}$. The total thicknesses of the Ge and Si layers observed using SIMS are in good agreement with the design. However, the avalanche region thickness is effectively reduced from 1.4 μm to approximately 1.3 μm . This reduction is possibly due to the diffusion of boron and arsenic during the growth of the Ge layer, and subsequent post-growth annealing which is used to reduce the dislocation density at the heterointerface. The boron peak at the interface between Ge and Si is possibly related to the misfit defects at the heterointerface preferentially trapping boron.

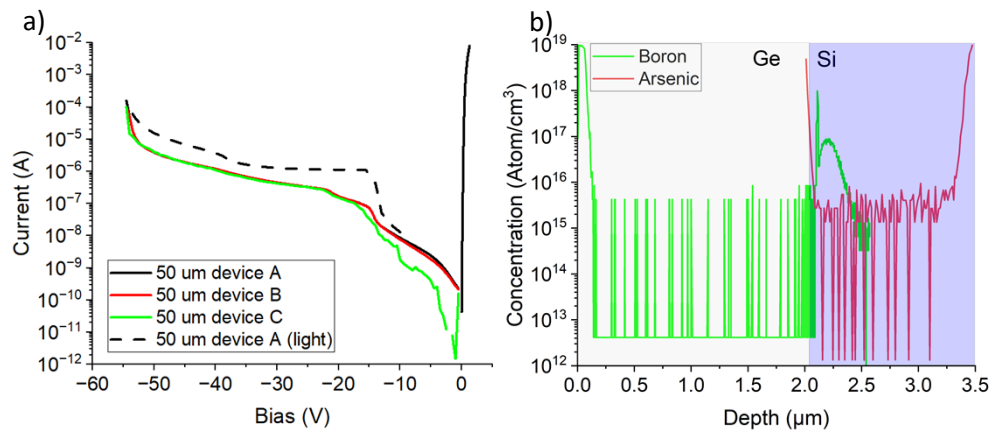


Fig. 2. a) Forward and reverse dark current (solid lines) in three different devices operated at room temperature (22°C). The photocurrent measurements (dashed line) were taken using a lock-in amplifier under 1550 nm wavelength illumination. b) SIMS elemental profiles of boron and arsenic measured from the top surface of Ge at 0 μm .

3.2. Photo-spectrum and responsivity

Figure 3(a) shows a comparison of the device responsivity at a reverse bias of 25 V observed when illuminated using a halogen light bulb source and a grating-based imaging monochromator (black line) and discrete laser wavelengths (marked as circles). The device optical responsivity was measured using a wavelength tuneable laser with a laser spot diameter of $\approx 10 \mu\text{m}$. The measured responsivity of a reference Ge photodiode on Si substrate with a similar absorption region thickness as our Ge-on-Si SAM-APD is 0.41 A/W under the same test conditions, giving us the primary responsivity (full details of the structure can be found in the [Supplement 1](#) section). The predicted responsivity of a Ge photodiode with a $2 \mu\text{m}$ thickness is 0.59 A/W at $\lambda = 1550 \text{ nm}$. The difference between the measured and predicted responsivity is likely due to a non-optimized anti-reflection coating and/or some recombination of photogenerated carriers at the $\text{Si}_x\text{N}_y/\text{Ge}$ interface and at Ge/Si interface. The Ge-on-Si device responsivity, shown in Fig. 3(b), was recorded under a wide range of reverse biases and surface-normal illumination conditions with light from the monochromator. This Ge-on-Si device shows a cut-off wavelength of 1730 nm at a high reverse bias (i.e. with gain). It can be seen that the cut-off wavelength extends with increased bias, which is strong evidence that the Franz-Keldysh (FK) effect [36,37] due to the direct bandgap, is present in this device which helps to extend the operation to longer wavelengths.

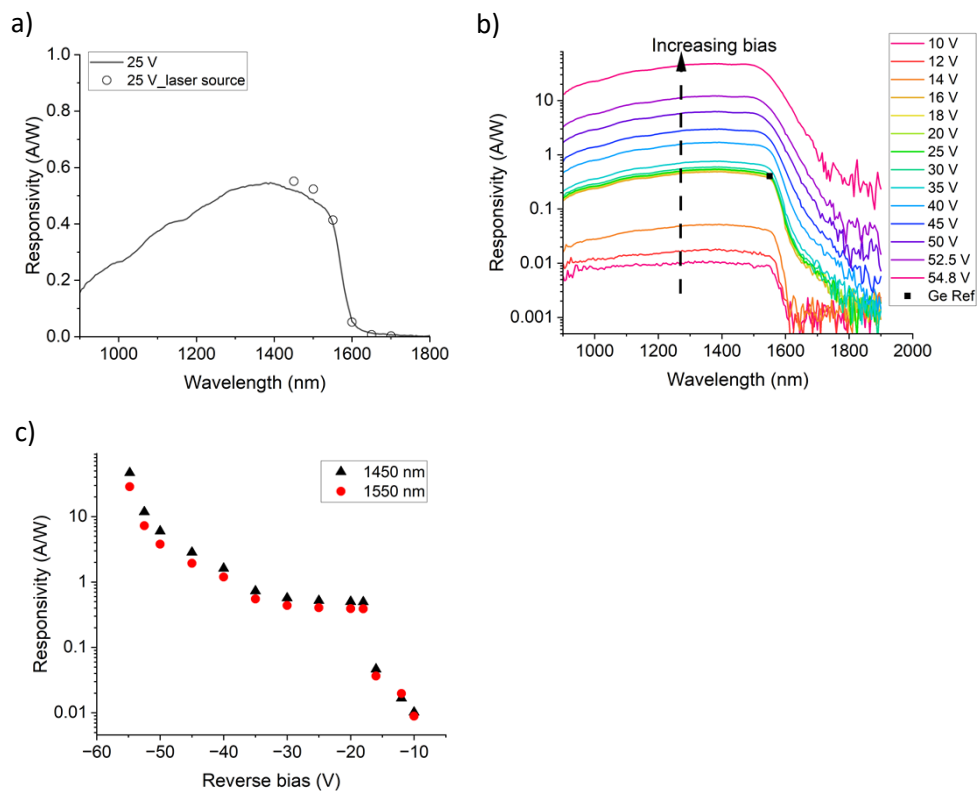


Fig. 3. a) The measured device responsivity using a white light and a grating-based monochromator at a reverse bias of 25 V (black line and markers). The circles denote discrete measurements made using a wavelength tuneable laser source. b) The device responsivity at room temperature under a wide range of reverse biases from 10 V to 54.8 V. The black square is the responsivity measured from a Ge reference diode. c) Measured responsivity at wavelengths of 1450 nm and 1550 nm.

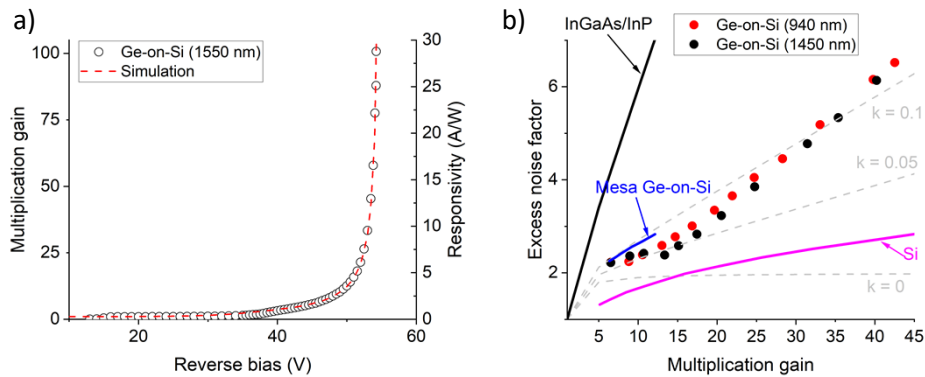


Fig. 4. a) A graph of the avalanche gain and responsivity vs reverse bias in the Ge-on-Si APD devices at 1550 nm wavelength illumination (circular markers). The dashed line corresponds to the RPL simulation with device layer thickness and doping as provided by SIMS. (b) Excess noise factor as a function of multiplication at wavelengths of 940 nm (red circular markers) and 1450 nm (black circular markers) from our Ge-on-Si APDs. The black, pink and blue solid lines are results from commercially available Si APDs [42], InGaAs/InP APDs [41] and a mesa Ge-on-Si APD [18], respectively. The dashed lines indicate McIntyre's local model for fixed k values of 0, 0.05 and 0.1, respectively.

Not only is the device responsivity amplified through the avalanche process in the silicon, the FK effect in the Ge absorber increases the overall device responsivity at wavelengths > 1600 nm. Figure 3(c) shows the responsivity comparison when illuminated at wavelengths of 1450 nm and 1550 nm. As this is a separate absorption (in Ge) and multiplication (in Si) design, there should be no wavelength dependence in the multiplication and excess noise for all wavelengths of light that are absorbed in the Ge layer as it is simply the electrons that enter the Si multiplication region.

3.3. Avalanche gain and excess noise

The avalanche gain in SAM-APD can be found by normalizing the measured SAM-APD's responsivity to the primary responsivity measured from the reference Ge photodiode (i.e.: 0.41 A/W). Figure 4(a) shows the maximum measurable avalanche gain, M of 101, at a wavelength of 1550 nm, which is two times higher than that previously reported with surface-illumination of Ge-on-Si APDs [19,35]. The high performance is related to the reduction in the likelihood of edge breakdown occurring through the use of the pseudo-planar geometry and a thicker Si multiplication layer. Gain values obtained through simulations using the random-path length (RPL) model [38] and the impact ionization coefficients of Si [39] are shown in Fig. 4(a) (red dashed line). The modelled and measured gain values are in very good agreement. The excess noise was measured in various devices using a transimpedance-amplifier-based circuit which has a centre frequency of 10 MHz and a bandwidth of 4.2 MHz [40]. Figure 4(b) shows a plot of the excess noise factor against avalanche gain at a wavelength of 940 nm (red markers) and 1450 nm (black markers) with an effective k value between 0.04 and 0.1. The theoretical excess noise factor given by McIntyre's local model [13] with a fixed k value of 0, 0.05 and 0.1 is included for comparison (dashed lines). The excess noise results achieved by illumination with a 940 nm wavelength light source are very similar when compared to longer wavelengths, suggesting wavelength independence of F in these SAM-APD devices. To the best of our knowledge, this is the lowest demonstrated F for short-wave infrared APDs fabricated on an Si platform. This low excess noise performance is due to our device having a thicker avalanche region leading to a smaller k value. For comparison, commercially available InGaAs/InP APDs show very high

excess noise (black line) [41]. Si APDs have been reported with lower excess noise characteristics (pink line), but this requires very high operating voltages due to a thick reach-through design [42] and the results are for wavelengths below the silicon bandgap of $\approx 1.1 \mu\text{m}$ in wavelength. The demonstrated excess avalanche noise from a mesa Ge-on-Si APD is $F = 2.5$ at an M of 10 for a wavelength of 1310 nm is also included in Fig. 4(b) (blue line) [18]. Details of device characterization methods can be found in the Supplement 1 section.

4. Discussion and conclusion

Table 1 shows the device performance of several surface-normal illuminated Ge-on-Si APDs and state-of-the-art III-V APDs for comparison. Although we used a thick layer design to achieve a better optical responsivity at a wavelength of 1550 nm and allow significantly higher gain operation, the dark current density remains similar to other Ge-on-Si APDs. We are not aware of any published experimental F at 1550 nm wavelength for APDs grown on Si substrates, however at the lower wavelength of 1310 nm, an F of 2.5 has previously been reported for the relatively low gain of $M = 10$ [18]. The excess noise was not reported in [18] for M greater than 12. Recently, an all-silicon microring APD demonstrated a responsivity of 65 A/W at a wavelength of 1310 nm and dark current of 6.5 μA at -7.36 V [43].

Table 1. Device performance of surface-normal illuminated APDs in the SWIR.

Reference	Platform	Absorber/ multiplication layer thickness	Breakdown voltage (V)	Dark current at 95% V_{bd} (A) and diameter	Primary responsivity (A/W)	Max gain	F ($M = 10$)	F ($M = 20$)
Present work	Si	2/1.4 μm	55	$\approx 5.7 \times 10^{-6}$ (50 μm)	0.41 ($\lambda = 1550 \text{ nm}$)	101	2.4	3.1
Ge-on-Si [18]	Si	1/0.6 μm	25	$\approx 2.5 \times 10^{-6}$ (30 μm)	0.78 (1310 nm)	32	2.5	N/A
Ge-on-Si [19]	Si	1.3/0.7 μm	26.1	$\approx 1.5 \times 10^{-6}$ (10 μm)	0.35 (1550 nm)	57	N/A	N/A
Ge-on-Si [20]	Si	1/0.7 μm	29.4	$\approx 3.5 \times 10^{-6}$ (30 μm)	0.3 (1550 nm)	39	N/A	N/A
Ge-on-Si [35]	Si	0.72/0.22 μm	56	$\approx 1 \times 10^{-6}$ (N/A)	0.08 (1550 nm)	57	N/A	N/A
All Si [42]	Si	N/A	150	$\approx 50 \times 10^{-12}$ (0.2 mm)	0.5 (800 nm)	100	1.5	2.1
InGaAs/ InP [41]	InP	N/A	55	$\approx 9 \times 10^{-8}$ (0.2 mm)	0.9 (1550 nm)	30	6	11
GaAsSb/ AlGaAsSb [44]	InP	0.89/0.2 μm	50	$\approx 7.8 \times 10^{-7}$ (50 μm)	0.5 (1550 nm)	130	1.52	2.48
GaAsSb/ AlGaAsSb [45]	InP	0.46/1.1 μm	67	$\approx 6.5 \times 10^{-7}$ (200 μm)	0.26 (1550 nm)	278	1.5	1.8
III-V on Si [46]	Si	1.1/0.25 μm	22	0.5×10^{-6} (20 μm)	0.54 (1550 nm)	22	3.52	5.56
InGaAs/InAlAs [47]	InP	1.0/0.2 μm	32	$\approx 2 \times 10^{-7}$ (30 μm)	0.48 (1550 nm)	120	2.8	4.5

Widely-used InGaAs/InP APDs can provide lower dark currents and higher primary responsivity at a wavelength of 1550 nm, but the limitation of large excess noise from InP prevents operation at $M > 15$. Recent reports suggest that the use of antimony such as in GaAsSb/AlGaAsSb APDs [44,45] can give much better performance than current InGaAs based APDs however this technology is not yet mature and manufacturing costs are significantly higher compared to Si based technologies. Furthermore integration with the electronics is likely to prove a challenge.

In conclusion, we have demonstrated a new type of surface-normal illumination Ge-on-Si APD design with a thicker absorption and multiplication layer for improving the main device performance parameters without sacrificing the dark current. The present design has the potential to be manufactured with high yield in a silicon foundry using standard silicon processes and provides the potential for integration with well-established and low-cost Si-based photonic and electronic devices. The APDs exhibit, to the best of our knowledge, the highest gain and the lowest excess noise factor on any Si photonics platform and are capable of operating at the strategically important wavelength of 1550 nm. Such a design can also easily be adapted into free-space applications. Furthermore, the demonstrated structure can be utilized in large APD arrays combined with well-established Si PICs for the next generation of sensing and imaging applications.

Funding. Engineering and Physical Sciences Research Council (EP/N003446/1, EP/S026428/1, EP/T00097X/1, EP/T001011/1, EP/W028166/1, EPN003225/1); Defence Science and Technology Laboratory (DSTLX-1000092774); Innovate UK (17706, 44835); Royal Academy of Engineering (CIET2021_123, RF201819-18-187); EC Horizon (grant number 101070700).

Acknowledgement. The authors would like to thank the staff of the James Watt Nanofabrication Centre at the University of Glasgow for help and support in the fabrication of the devices.

Disclosures. The authors declare no conflict of interest.

Data availability. Data underlying the results presented in this paper are available from Xin Yi (xin.yi@hw.ac.uk) upon reasonable request.

Supplemental document. See [Supplement 1](#) for supporting content.

References

1. Y. Yuan, B. Tossoun, Z. Huang, *et al.*, "Avalanche photodiodes on silicon photonics," *J. Semicond.* **43**(2), 021301 (2022).
2. M. Nada, F. Nakajima, T. Yoshimatsu, *et al.*, "High-speed III-V based avalanche photodiodes for optical communications—the forefront and expanding applications," *Appl. Phys. Lett.* **116**(14), 140502 (2020).
3. J. C. Campbell, J. P. R. David, and S. R. Bank, "Sb-based low-noise avalanche photodiodes," *Photonics* **10**(7), 715 (2023).
4. Y. Shi, X. Li, G. Chen, *et al.*, "Avalanche photodiode with ultrahigh gain–bandwidth product of 1,033 GHz," *Nat. Photonics* (2024).
5. S. Assefa, F. Xia, and Y. A. Vlasov, "Reinventing germanium avalanche photodetector for nanophotonic on-chip optical interconnects," *Nature* **464**(7285), 80–84 (2010).
6. A. H. Jones, S. D. March, S. R. Bank, *et al.*, "Low-noise high-temperature AlInAsSb/GaSb avalanche photodiodes for 2- μ m applications," *Nat. Photonics* **14**(9), 559–563 (2020).
7. R. H. Hadfield, J. Leach, F. Fleming, *et al.*, "Single-photon detection for long-range imaging and sensing," *Optica* **10**(9), 1124–1141 (2023).
8. S. Royo and M. Ballesta-Garcia, "An overview of lidar imaging systems for autonomous vehicles," *Appl. Sci.* **9**(19), 4093 (2019).
9. A. M. Wallace, A. Halimi, and G. S. Buller, "Full waveform LiDAR for adverse weather conditions," *IEEE Trans. Veh. Technol.* **69**(7), 7064–7077 (2020).
10. J.-E. Joo, M.-J. Lee, and S. M. Park, "A CMOS optoelectronic receiver IC with an on-chip avalanche photodiode for home-monitoring LiDAR Sensors," *Sensors*, **21**(13), 4364 (2021).
11. K. Kuzmenko, P. Vines, A. Halimi, *et al.*, "3D LIDAR imaging using Ge-on-Si single photon avalanche diode detectors," *Opt. Express* **28**(2), 1330–1344 (2020).
12. J. C. Campbell, "Recent advances in telecommunications avalanche photodiodes," *J. Lightwave Technol.* **25**(1), 109–121 (2007).
13. R. J. McIntyre, "Multiplication noise in uniform avalanche diodes," *IEEE Trans. Electron Devices* **ED-13**(1), 164–168 (1966).
14. R. B. Emmons, "Avalanche-photodiode frequency response," *J. Appl. Phys.* **38**(9), 3705–3714 (2004).
15. A. Arnulf, J. Bricard, E. Curé, *et al.*, "Transmission by haze and fog in the spectral region 0.35 to 10 microns*," *J. Opt. Soc. Am.* **47**(6), 491–498 (1957).
16. R. E. Bird, R. L. Hulstrom, and L. J. Lewis, "Terrestrial solar spectral data sets," *Sol. Energy* **30**(6), 563–573 (1983).
17. J. Michel, J. Liu, and L. C. Kimerling, "High-performance Ge-on-Si photodetectors," *Nat. Photonics* **4**(8), 527–534 (2010).
18. Y. Kang, H.-D. Liu, M. Morse, *et al.*, "Monolithic germanium/silicon avalanche photodiodes with 340 GHz gain–bandwidth product," *Nat. Photonics* **3**(1), 59–63 (2009).

19. G. Kim, S. Kim, S. A. Kim, *et al.*, “NDR-effect vertical-illumination-type Ge-on-Si avalanche photodetector,” *Opt. Lett.* **43**(22), 5583–5586 (2018).
20. N. Duan, T.-Y. Liow, A. E.-J. Lim, *et al.*, “310 GHz gain-bandwidth product Ge/Si avalanche photodetector for 1550 nm light detection,” *Opt. Express* **20**(10), 11031–11036 (2012).
21. S. Wu, H. Zhou, L. He, *et al.*, “Ge-on-Si avalanche photodiodes with photon trapping nanostructures for sensing and optical quantum applications,” *IEEE Sens. J.*, **1** (2023).
22. N. J. D. Martinez, C. T. Derose, R. W. Brock, *et al.*, “High performance waveguide-coupled Ge-on-Si linear mode avalanche photodiodes,” *Opt. Express* **24**(17), 19072–19081 (2016).
23. S. A. Srinivasan, M. Berciano, P. D. Heyn, *et al.*, “27 GHz silicon-contacted waveguide-coupled Ge/Si avalanche photodiode,” *J. Lightwave Technol.* **38**(11), 3044–3050 (2020).
24. S. A. Srinivasan, J. Lambrecht, D. Guermandi, *et al.*, “56 Gb/s NRZ O-band hybrid BiCMOS-Silicon photonics receiver using Ge/si avalanche photodiode,” *J. Lightwave Technol.* **39**(5), 1409–1415 (2021).
25. D. Benedikovic, L. Viro, G. Aubin, *et al.*, “40 Gbps heterostructure germanium avalanche photo receiver on a silicon chip,” *Optica* **7**(7), 775–783 (2020).
26. Z. Huang, C. Li, D. Liang, *et al.*, “25 Gbps low-voltage waveguide Si-Ge avalanche photodiode,” *Optica* **3**(8), 793–798 (2016).
27. Y. Xiang, H. Cao, C. Liu, *et al.*, “High-speed waveguide Ge/Si avalanche photodiode with a gain-bandwidth product of 615 GHz,” *Optica* **9**(7), 762–769 (2022).
28. B. Wang, Z. Huang, Y. Yuan, *et al.*, “64 Gb/s low-voltage waveguide SiGe avalanche photodiodes with distributed Bragg reflectors,” *Photonics Res.* **8**(7), 1118–1123 (2020).
29. P. Vines, K. Kuzmenko, J. Kirdoda, *et al.*, “High performance planar germanium-on-silicon single-photon avalanche diode detectors,” *Nat. Commun.* **10**(1), 1086 (2019).
30. L. Ferre-Llin, J. Kirdoda, F. E. Thorburn, *et al.*, “High sensitivity Ge-on-Si single-photon avalanche diode detectors,” *Opt. Lett.* **45**(23), 6406–6409 (2020).
31. F. Thorburn, X. Yi, Z. M. Greener, *et al.*, “Ge-on-Si single-photon avalanche diode detectors for short-wave infrared wavelengths,” *Journal of Physics: Photonics* **4**, 012001 (2022).
32. X. Yi, Z. Greener, F. Fleming, *et al.*, “Afterpulsing in Ge-on-Si single-photon avalanche diodes,” *IEEE Photonics Technol. Lett.* **35**(17), 959–962 (2023).
33. H. Ye and J. Yu, “Germanium epitaxy on silicon,” *Sci. Technol. Adv. Mater.* **15**(2), 024601 (2014).
34. C. L. Hsin and C. H. Chou, “Buffer-Free Ge/Si by rapid melting growth technique for separate absorption and multiplication avalanche photodetectors,” *IEEE Electron Device Lett.* **40**(6), 945–948 (2019).
35. X. Liu, X. Li, Y. Li, *et al.*, “Three-terminal germanium-on-silicon avalanche photodiode with extended p-charge layer for dark current reduction,” *Photonics Res.* **10**(8), 1956–1963 (2022).
36. M. Schmid, M. Kaschel, M. Gollhofer, *et al.*, “Franz-Keldysh effect of germanium-on-silicon p-i-n diodes within a wide temperature range,” *Thin Solid Films* **525**, 110–114 (2012).
37. M. Oehme, K. Kostecky, M. Schmid, *et al.*, “Franz-Keldysh effect in GeSn pin photodetectors,” *Appl. Phys. Lett.* **104**(16), 161115 (2014).
38. D. S. Ong, K. F. Li, G. J. Rees, *et al.*, “A simple model to determine multiplication and noise in avalanche photodiodes,” *J. Appl. Phys.* **83**(6), 3426–3428 (1998).
39. R. Van Overstraeten and H. De Man, “Measurement of the ionization rates in diffused silicon p-n junctions,” *Solid-State Electron.* **13**(5), 583–608 (1970).
40. K. F. Li, D. S. Ong, J. P. R. David, *et al.*, “Avalanche multiplication noise characteristics in thin GaAs p⁺-i-n⁺ diodes,” *IEEE Trans. Electron Devices* **45**(10), 2102–2107 (1998).
41. “Hamamatsu Photonics K.K. InGaAs APD G8931 series,” <https://www.hamamatsu.com/eu/en/product/optical-sensors/apd/ingaas-apd/G8931-20.html>.
42. “Hamamatsu K.K. Photonics Si APD S10341 series,” https://www.hamamatsu.com/content/dam/hamamatsu-photonics/sites/documents/99_SALES_LIBRARY/ssd/s10341_series_kapd1030e.pdf.
43. Y. Peng, Y. Yuan, W. V. Sorin, *et al.*, “All-silicon microring avalanche photodiodes with a >65 A/W response,” *Opt. Lett.* **48**(5), 1315–1318 (2023).
44. Y. Cao, T. Blain, J. D. Taylor-Mew, *et al.*, “Extremely low excess noise avalanche photodiode with GaAsSb absorption region and AlGaAsSb avalanche region,” *Appl. Phys. Lett.* **122**(5), 051103 (2023).
45. S. Lee, X. Jin, H. Jung, *et al.*, “High gain, low noise 1550 nm GaAsSb/AlGaAsSb avalanche photodiodes,” *Optica* **10**(2), 147–154 (2023).
46. Y. Yuan, D. Jung, K. Sun, *et al.*, “III-V on silicon avalanche photodiodes by heteroepitaxy,” *Opt. Lett.* **44**(14), 3538–3541 (2019).
47. W. Wang, J. Yao, L. Li, *et al.*, “High-speed InAlAs digital alloy avalanche photodiode,” *Appl. Phys. Lett.* **123**(19), 191102 (2023).